Synchronous amplitude and time control for an optimum dynamic range variable photonic delay line

Nabeel A. Riza and Nicholas Madamopoulos

A synchronous-amplitude-controlled and time-delay-controlled photonic controller for phased-array antenna applications is proposed and demonstrated. Amplitude control is based on a variable optical attenuator system that operates in synchronism with the photonic delay line (PDL). This amplitude control system can provide both the signal calibration for the different PDL channels and settings required for driving the antenna elements of a phased-array radar and the optimum optical power levels that impinge on the photodetector for optimum fiber-optic-link performance. Various variable amplitude control modules based on ferroelectric liquid crystals, polymer-dispersed liquid crystals, and photoconductive devices are proposed. We show that the dynamic range loss due to a switched-PDL inherent structure loss can be compensated when we control the optical power from the laser, using the synchronous optical attenuation system. For the first time to our knowledge, full dynamic range loss compensation is demonstrated for an external-modulation-fed 3-bit switched PDL with a structure optical insertion loss of 5.5 dB. A compression dynamic range of 158 dB·Hz was measured at 6 GHz, and a spurious free dynamic range of 111 dB·Hz$^{2/3}$ was estimated. Feasibility of the dynamic range compensation technique for multichannel, higher-insertion-loss PDL systems is discussed.

OCIS codes: 060.2360, 230.3720, 350.4010, 280.5110.

1. Introduction

In recent years different photonic approaches have been proposed and experimentally demonstrated for the implementation of variable photonic delay lines (PDL's) for phased-array antenna applications.[1] One of the main issues with variable PDL's and their use in practical phased-array antenna applications is their insertion loss. In the past few years we have been developing switched PDL's based on bulk optics and ferroelectric liquid-crystal (FLC) polarization switches. We have demonstrated switching times of 35 μs (Ref. 2) and within channel rf leakage noise suppression of less than −75 dB for the 16 different settings of a 4-bit PDL.[3] Radio-frequency insertion loss numbers of 3.6 dB/bit have been demonstrated[3] and are expected to be reduced at <2.8 dB/bit with improved FLC devices. Nevertheless, this PDL loss, in conjunction with the limited fiber-optic- (FO-) link gain, especially at high rf frequencies (e.g., >2 GHz), is sometimes the limiting factor in terms of compression dynamic range (CDR), spurious free dynamic range (SFDR), and noise figure (NF) of the photonic system. These factors are important for phased-array antenna applications and hence are the subject of this paper with respect to PDL's.

Over the past few years the use of analog FO links for phased-array antennas has been explored.[4] Currently, external modulation FO links give a greater degree of freedom to the optical engineer to obtain optimized performance. Thus an external modulation FO link gives better performance characteristics for analog applications compared with direct modulation FO links.[5,6] Externally modulated links compared with directly modulated links have demonstrated higher gains,[6,7] higher modulation frequencies[8] and bandwidths,[7,8] and higher dynamic ranges.[9] Specifically, a gain of +11 dB has been reported with a 22-MHz bandwidth.[6] Frequencies of 20 GHz with a 6.6-GHz bandwidth[8] have been demonstrated, and maximum CDR's of 160 dB·Hz and SFDR's of 117 dB·Hz$^{2/3}$ have been reported for an external modulation link at 870–930 MHz.[9] With a balanced detection scheme for a 3-GHz FO

The authors are with the School of Optics and the Center for Research and Education in Optics and Lasers, University of Central Florida, P.O. Box 162700, 4000 Central Florida Boulevard, Orlando, Florida. N. A. Riza's e-mail address is riza@creol.ucf.edu.

Received 14 September 1998; revised manuscript received 30 November 1998.

0003-6935/99/112309-10$15.00/0

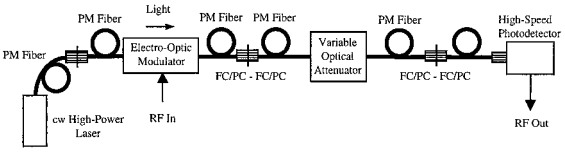

Fig. 1. Typical experimental setup for the externally modulated FO link. A FO attenuator is used to adjust the optical power impinging on the photodetector. PM, polarization maintaining; cw, continuous wave.

link, a CDR of 168.4 dB·Hz and a SFDR of 119.5 $dB \cdot Hz^{2/3}$ have also been reported.[10] Thus the preferred choice at present for phased-array antenna applications is external modulation FO links.

Externally modulated links typically include a diode-pumped solid-state laser with an optical output power of ~200 mW or more, a Mach–Zehnder integrated electro-optic modulator capable of handling 200 mW or more of continuous-wave (cw) optical power, and a fast photodetector that usually has a maximum acceptable optical power of 3–5 mW for operation at frequencies >1 GHz. This 3–5-mW limitation is due to the nonlinear response of the photodiode at high-optical-power densities. The low-optical-input-power photodetector is currently the limiting factor for low or negative FO-link gains operating at frequency bands of a few gigahertz. Gain is considered in the general sense where negative gain means loss. The lower levels of acceptable optical power on the photodetector are due to the small photodetector area (e.g., approximately 10–20 μm in diameter) required so that the corresponding capacitance does not limit the link operational bandwidth.[7] Thus the available optical power from the laser needs to be attenuated before it reaches the receiver. This can be done with a FO attenuator as shown in Fig. 1. There are two possible FO attenuator positions in the FO link. The first is before the electro-optic modulator, and the second is after it. Since the modulator is capable of handling the laser optical power, we chose to place the FO attenuator after the modulator. For reasons that are discussed below (Section 4) this FO attenuator position gives a better performance to the FO link in terms of noise issues. Typical FO-link gain numbers obtained with a diode-pumped Nd:YAG laser (λ = 1319 nm), a Uniphase Telecommunications Products (UTP) Mach–Zehnder analog modulator, and a Lasertron fast photodetector for operation in the 3–6-GHz band is approximately −30 dB. Preamplifiers and/or postamplifiers can be used to improve the FO link gain, but this may affect the NF and/or the dynamic range of the link.[11]

To use a FO link for phased-array antenna applications, a variable PDL is inserted after the FO attenuator. The optical insertion loss of the PDL will lower the optical power detected at the photodetector and thus will further reduce the FO link gain. Thus a limited dynamic range will be obtained for the FO-link–PDL system. This is particularly important in the receive mode of the photonic beam former, as signals coming from the antenna elements are lower in power. Note also that for most advanced phased-array applications the signals driving the antenna elements are required to be of equivalent amplitudes. Thus a balanced loss performance between the different settings of a PDL is also a critical system-design need. Recently we proposed a balanced insertion loss PDL bit architecture that has equal loss for each PDL bit setting.[12] Nevertheless, small insertion loss variation due to the different optical losses of the optical components or due to the loss variation throughout their entire active area may lead to an insertion loss variation for the different PDL channels and/or settings. Thus the use of the optical attenuator is required not only for providing the optimum optical power for maximum dynamic range but also for providing equal optical signal amplitudes for all different PDL settings and channels.

In this paper we propose an optical amplitude control system that operates in synchronism with the PDL to provide the necessary signal amplitude calibration and the important dynamic range loss compensation that produces the optimized rf performance of our FO-link–PDL system.[3] We also demonstrate how this optical attenuation system can be used to obtain maximum rf dynamic range for a FO-link–PDL system made up of commercially available components. The proposed signal amplitude calibration and dynamic range loss compensation technique is not limited to our PDL design and technology and can also be used with alternative PDL approaches. To our knowledge, our amplitude controlled approach gives the highest FO-link dynamic range ever reported with use of a switched-PDL system.[13–18] The previously reported high dynamic range (160 dB·Hz) has been demonstrated with nonswitched FO PDL's.[19]

2. Synchronous Signal Calibration and Dynamic Range Loss Compensation Technique

The proposed synchronous signal calibration and dynamic range loss compensation method is based on the high optical power available from the laser source and on an electrically controlled optical attenuator after the electro-optic modulator. This attenuator is set such that the incident optical power after propagation and attenuation through the PDL is at levels required from the detector for maximum photodetected dynamic range. Figure 2 shows such a configuration where the optical attenuator is computer controlled. For PDL calibration purposes on a day-to-day basis the rf power splitter sends a small portion of the rf power to the power meter, and, with the help of a computer and a database, the appropriate feedback signal is sent to the attenuator for fine control. Because the PDL loss for each bit setting is known, the attenuator settings are also known *a priori*, and thus the appropriate attenuator setting is applied by means of an electronic signal that controls the high-speed optical attenuator. Advanced phased-array antenna applications require switching times of a few microseconds. Currently the FO attenua-

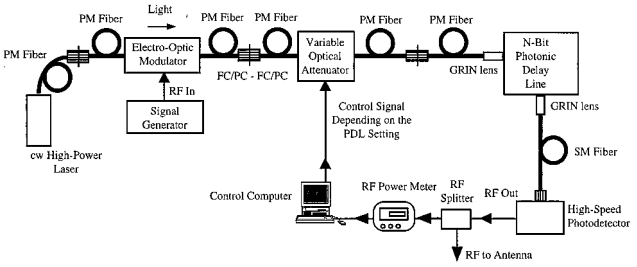

Fig. 2. Dynamic range loss compensation method based on high-speed electronic control of the variable optical attenuator in synchronous control with the PDL settings.

tors available on the market are limited to slower switching times (e.g., 200-ms full span scanning for a 30-dB attenuation range).[20] Thus a faster switching speed optical attenuator is required.

Figure 3(a) shows the basic structure of a digital control, high-speed, binary design, variable optical attenuator that operates in synchronism with the variable PDL. Each attenuator module has two possible settings: the zero attenuation (A_0) setting and the A_i attenuation setting, where $i = 1, 2, \ldots, N$. This is achieved by use of two light propagation paths with different optical losses in the attenuator module. One path gives the zero attenuation (A_0), and the other one gives the A_i attenuation. The attenuation modules are arranged in a cascade switched configuration, with each module having twice the attenuation of the previous one; i.e., $A_{i+1} = 2 \times A_i$. Thus the cascade of these binary attenuation modules provides the desired attenuation range. Note that since polarization-maintaining fibers are used in the system configuration (see Fig. 2), a polarization-dependent high-speed optical attenuator can be used. Similar to our PDL designs, one polarization-based attenuator uses high-speed (e.g., 35 μs) binary FLC polarization switching devices and polarization beam splitters (PBS's) to route the optical signal to one of the two possible paths in the attenuator module.[21] Figure 3(b) shows a multichannel design with attenuation plates that can be simple neutral-density filters designed to provide the desired attenuation. Another option is to use fixed-power polarization rotators such as half-wave retarders or voltage-controlled birefringent mode nematic liquid-crystal devices. These polarization rotators are set such that they rotate the incident linear polarization by a predefined angle. Then, owing to the output PBS, only one polarization component (e.g., horizontal polarization) of the linearly polarized light will be transmitted through the PBS toward the output of the attenuator module. Thus by adjustment of the degree of rotation of the incident polarized light the desired attenuation can be realized. The first polarization switch labeled S in Fig. 3(b) is used to control the state of polarization of the input light to the single-bit module. Depending on this state of polarization, the light can follow either the zero attenuation path A_0 or the A_i path. The second switch S in the module and the polarizer in the subsequent module are used to suppress any polarization leakage that is due to the switches and to the PBS's. Note that the polarization rotator approach gives greater flexibility to the optical engineer compared with the neutral-density filter approach for obtaining the desired attenuation, since the attenuation can be fine-tuned to the desired level by adjustment of either the voltage applied to the NLC device or the orientation of the optical axis of the half-wave retarder.

Another FLC-based optical attenuation system is depicted in Fig. 3(c). With this approach, FLC devices operate in the binary phase mode and act as beam profile spoilers. This can be achieved by placement of the FLC device such that the optical axis is switching symmetrically around the output polarizer axis, and thus the output signal is phase modulated with a phase factor of π.[22,23] By individual control of the axis orientation of the two-dimensional (2-D) FLC-pixelated array, areas with alternating 0 and π phases can be realized. Thus a variable fringe spacing 0–π phase 2-D grating can be realized that can cause phase perturbations on the beam phase front. In general the 0–π phase distribution can have any configuration and not necessarily a gratinglike one. Single-mode fiber-coupling efficiency with a FO collimator approach is highly dependent on the wavefront characteristics of the incident wave.[24,25] Thus the 2-D phase perturbation can affect the coupling efficiency of the beam into the FO collimator. Hence an attenuated optical signal can be obtained by proper adjustment of the phase perturbation distribution across the incident beam.

An alternative gray-scale optical attenuator option is shown in Fig. 3(d). This design is based on holographic polymer-dispersed liquid-crystal (PDLC) devices. PDLC devices can be used as variable diffraction efficiency voltage-controlled gratings and have been reported to have switching speeds of <50 μs.[26] The excess light in a PDLC device can be rejected into the first diffraction order. Thus the right amount of optical attenuation can be accomplished. Compared with the binary design, this approach gives a reduced size and reduced excess optical loss attenuator, as it has only one attenuation stage. Nevertheless, it requires a precise analog voltage controller for driving the PDLC device.

The above-mentioned optical attenuator architectures perform rf signal attenuation in the optical domain, as the optical signal propagates through the PDL system. A different optical architecture for obtaining the important signal calibration is based on an N-bit optically controlled microwave photoconductive attenuator.[27,28] This approach is based on the photoconductive effect in coplanar waveguide (CPW) microwave transmission lines, and the attenuation is applied directly on the microwave signal by optical means. The photodetected microwave signal is transmitted to the antenna element by use of a microwave transmission line fabricated on a silicon photoconductive substrate. When optical beams hit the transmission line, hole–electron pairs are generated.

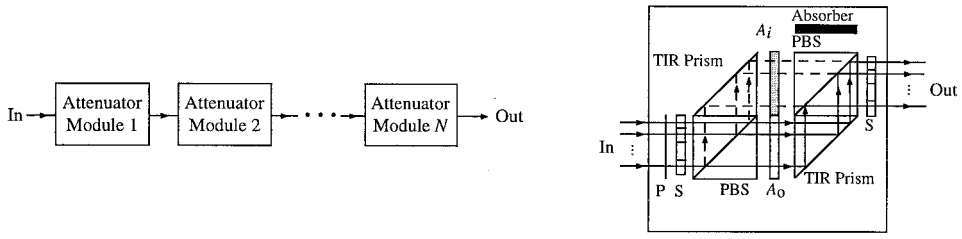

(a) (b)

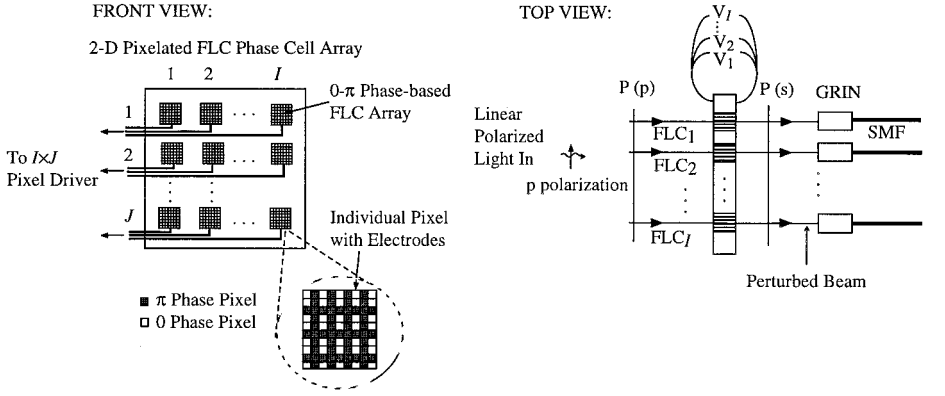

(c)

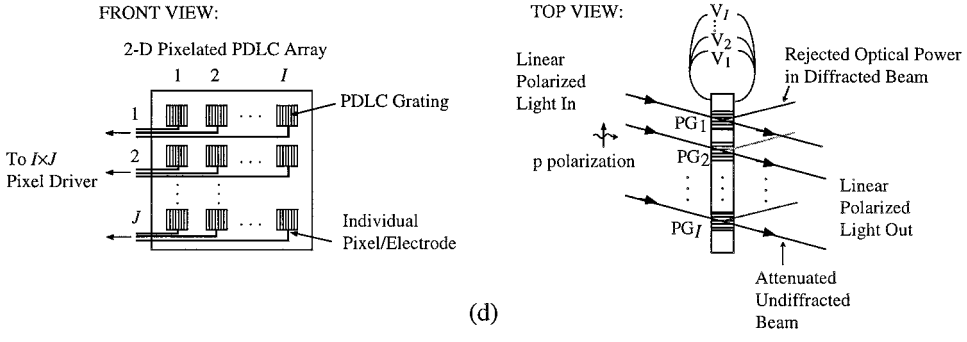

(d)

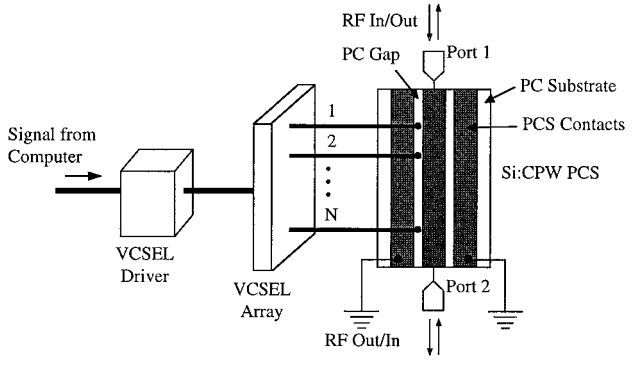

(e)

Fig. 3. (a) Basic design of a high-speed, variable optical attenuator that operates in synchronism with the variable PDL. The variable optical attenuator consists of a cascade of binary attenuator modules. (b) The high-speed, variable optical attenuator based on fast FLC polarization switching devices and polarization beam-splitter cubes (TIR, total internal reflection; P, polarizer; S, polarization switch; A_i, attenuation plate with attenuation value A_i; A_0, attenuation plate with zero attenuation). (c) Phase-perturbation-based optical attenuator with $I \times J$ independently, $0-\pi$ phase, controlled FLC arrays (SMF, single-mode fiber; GRIN, gradient-index lens). (d) Single-stage gray-scale optical attenuator based on a holographic PDLC device with $I \times J$ independently controlled variable diffraction efficiency programmable gratings (PG's). (e) The N-bit electro-optic attenuator based on the photoconductive effect. The 2-D VCSEL array is used to activate each photoconductive bit. (Si:CPW PCS, coplanar microwave waveguide on a photoconductive silicon substrate).

Thus, a solid-state plasma is created in the semiconductor. The interaction of this plasma with the propagating microwave signal provides the rf attenuation. It has been shown that if the transmission lines are illuminated by N control beams with different optical powers that follow a binary pattern, then an N-bit attenuator can be implemented. Figure 3(e) shows a possible design for the photoconductive-effect-based attenuator. The optical beams incident on the photoconductive material can be from a VCSEL array.[27] The VCSEL structure contains many individual laser diodes that can be independently addressed with a 2-D VCSEL driver and interface. The individual lasers can be computer controlled to be either ON or OFF depending on the desired attenuation level. In the ON case the individual laser can be arranged to have a binary power pattern. Thus, by independently turning ON and OFF the lasers, we can realize an N-bit rf attenuator.

In the following paragraphs we describe and test a method for dynamic range loss compensation in a FO link without a rf amplifier.

3. Experimental Demonstration of the Signal Calibration and Dynamic Range Loss Compensation Technique

The optical source used in our experiments was a diode-pumped Nd:YAG laser at 1319 nm from ATX Telecom Systems, Inc. The electro-optic modulator is a UTP $LiNbO_3$ Mach–Zehnder analog modulator biased at quadrature, and the detector is a Lasertron QRX-51-053 receiver. A manually controlled OZ-Optics FO attenuator is used to simulate an electronically controlled high-speed optical attenuator. First, the performance of the externally modulated FO link without the PDL at 6 GHz is tested. The optical attenuator in the FO link was adjusted so that an optical power of 3 mW is incident on the photodetector. This 3-mW optical power is the optimum optical power for our Lasertron receiver. The FO link exhibits a -32.16-dB rf gain (or a 32.16-dB rf loss) at 6 GHz. Figure 4 shows the measured FO link fundamental-output versus the link fundamental-input plot at a frequency of 6 GHz. The 1-dB compression output power is -11.26 dBm at a $+20.9$-dBm input power. As the 1-dB compression point we define the point where the conversion loss is increased by 1 dB. The noise-floor power spectral density of the FO link was measured at -139.2 dBm/kHz (or -169.2 dBm/Hz). Thus a compression dynamic range (CDR) of 127.8 dB at 1-kHz bandwidth (or 157.8 dB·Hz) is calculated. The CDR is a measure of the variation of the signal levels that can be carried by the link. Typically, it is defined as the difference (in decibels) between the maximum detectable power in the linear regime (defined as being 1 dB higher than the 1-dB compression output power) to the minimum detectable power (usually defined as being equal to the noise floor).[9] The CDR is also often called the signal-to-noise ratio (SNR) of the FO link. The 1-dB input power compression point is found to be close to the theoretically expected one given by UTP for their modulator.[29]

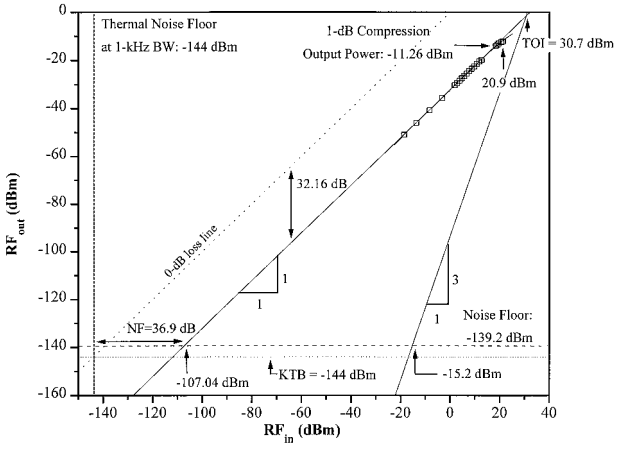

Fig. 4. FO-link fundamental and two-tone intermodulation distortion output versus the link fundamental input at 6 GHz (resolution bandwidth 1 kHz).

The rms V_π of the UTP modulator is 4.3 V, which corresponds to a P_π of 25.7 dBm. P_π is defined as the rf power required for generating V_π.[29] The 1-dB input power compression point ($P_{\text{in},-1\text{ dB}}$) is then estimated by[29,30]

$$P_{\text{in},-1\text{ dB}} = P_\pi - 3.9\text{ dB} = 21.6\text{ dBm}. \quad (1)$$

The third-order intermodulation (TOI) point, defined as the point where the fundamental signal and third-order intermodulation product powers are equal, can also be calculated with the following equation to be[29,30]

$$P_{\text{in,TOI}} = P_\pi + 5.1\text{ dB} = 30.7\text{ dBm}. \quad (2)$$

With the $P_{\text{in,TOI}}$ and the fact that the two-tone intermodulation distortion plot has a slope of 3, the expected two-tone intermodulation distortion link output versus the link fundamental input power can be plotted (Fig. 4). Hence a potential SFDR of 91.8 $\text{dB}\cdot\text{kHz}^{2/3}$ or (111.8 $\text{dB}\cdot\text{Hz}^{2/3}$) is estimated. The SFDR is defined as the maximum difference between the noise floor and the fundamental output that produces distortion terms of equal amplitude to the noise floor. The NF of the FO link is also measured at 36.9 dB. The NF is the degradation in the SNR caused by transmission through the link when the input noise is thermal noise at 290 K and is defined as[31]

$$\text{NF} = 10\log\frac{\text{input SNR}}{\text{output SNR}} = 10\log\frac{S_i/N_i}{S_o/N_o}, \quad (3)$$

where S_o and S_i are the output and the input signal powers, respectively. N_o is the available output noise power, and $N_i = KTB$ is the available input noise power from the generator, at temperature $T =$ 290 K and with bandwidth B. K is the Boltzmann's constant. When we rearrange Eq. (3), the NF can also be expressed as

$$\text{NF} = P_{\text{noise floor}} - [-174 + 10\log(B)] - G, \quad (4)$$

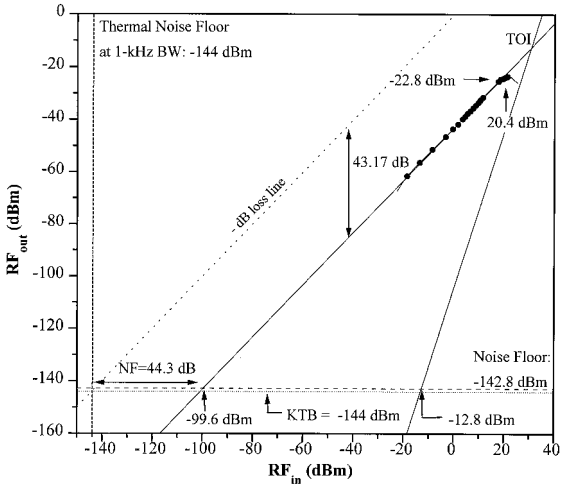

Fig. 5. FO-link fundamental and two-tone intermodulation distortion output versus the link fundamental input at 6 GHz when the PDL is inserted in the optical path (resolution bandwidth 1 kHz).

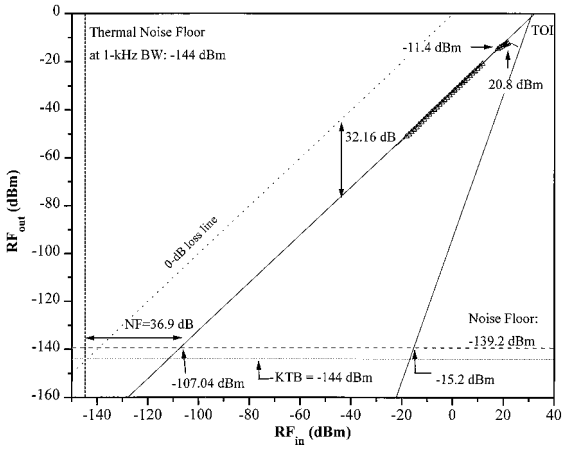

Fig. 6. FO-link fundamental and two-tone intermodulation distortion output versus the link fundamental input at 6 GHz when the dynamic range loss recovery technique is used (resolution bandwidth 1 kHz).

where $P_{\text{noise floor}}$ is the noise-floor power measured in decibels referenced to milliwatts at a specific bandwidth B, -174 dBm is the available thermal noise at the input of the link at a temperature of 290 K and a 1-Hz bandwidth, and G is the gain of the FO link in decibels.

When the PDL is inserted into the externally modulated link path by use of fiber-to-free space coupling optics (e.g., gradient-index or GRIN lens fiber-optic collimators), an extra rf loss is expected. The FO attenuator remains in its previous setting; hence the input optical power to the PDL was 3 mW. Our 3-bit PDL had best and worst optical insertion losses of 5.5 dB and 5.7 dB, respectively. Using our optical attenuator, we equalized the optical insertion loss for all different settings at a 5.5 dB. Thus the rf gain of the FO link is now expected to be $-32.16 + 2(-5.5) = -43.16$ dB. Indeed, Fig. 5 shows a measured rf FO-link gain of -43.17 dB at 6 GHz. Figure 5 also shows the measured FO-link–PDL system fundamental output and the expected two-tone intermodulation distortion link output versus the link fundamental input. We assume that the effect of the PDL in the two-tone intermodulation distortion would be only an attenuation of the output signal. This is assumed, because the third-order intermodulation products are generated by the nonlinearities in the external modulator. Thus the PDL only attenuates the third-order intermodulation product power by the same amount as the fundamental, i.e., by the amount that the gain decreases. The 1-dB compression output power is -22.8 dBm at $+20.4$ dBm input power. We measured a noise-floor power spectral density of -142.8 dBm/kHz (or -172.8 dBm/Hz). Thus the CDR is 120 dB·kHz (or 150 dB·Hz). This FO-link gain (which is lower by -11.01 dB, affects the CDR, which now is 8 dB lower than in the previous case. The lower noise floor observed in this case is due to the lower optical power impinging onto the photodetector and thus to the lower photodetector shot noise, which is the dominant source of noise in our externally modulated FO link. The potential SFDR can also be estimated as above at 86.8 dB·kHz$^{2/3}$ (or 106.8 dB·Hz$^{2/3}$). The NF of the system is calculated with Eq. (4) at 44.3 dB, a 7.4-dB degradation compared with the previous case.

The next step was to reduce the optical attenuator setting by 5.5 dB so that the PDL optical insertion loss is balanced and the light incident on the photodetector is again 3 mW. The measured FO-link–PDL system fundamental output and the expected two-tone intermodulation distortion link output versus the fundamental link input are plotted in Fig. 6. The compensation of the PDL optical insertion loss by an equal amount of reduction in the optical attenuation of input optical power to the PDL has an effect such that the FO-link gain and the CDR reach their links without PDL values of -32.16 dB and -127.8 dB, respectively, at a 1-kHz bandwidth (or 157.8 dB·Hz). The 1-dB compression output power is -11.4 dBm at a 20.8-dBm input power. The noise-floor power spectral density is -139.2 dBm/kHz (or -169.2 dBm/Hz), and the NF and the SFDR also obtain their links without PDL values.

The experiment was repeated at 3 GHz to test the wideband capability of the FO link. Figure 7 shows the fundamental output and the expected two-tone intermodulation distortion link output versus the fundamental link input of the FO link at 3 GHz. A CDR of 123.05 dB·kHz (or 153.05 dB·Hz) and a SFDR of 88 dB·kHz$^{2/3}$ (or 108 dB·Hz$^{2/3}$) was obtained. Figure 8 shows the linear and the third-order intermodulation distortion responses of the FO link with the PDL. The insertion loss of the PDL reduces both the CDR and the SFDR at 116.5 dB·kHz (or 146.5 dB·Hz) and 83.5 dB·kHz$^{2/3}$ (or 103.5 dB·Hz$^{2/3}$), respectively. Figure 9 shows the linear and the third-order intermodulation distortion responses of the FO link with the PDL when the

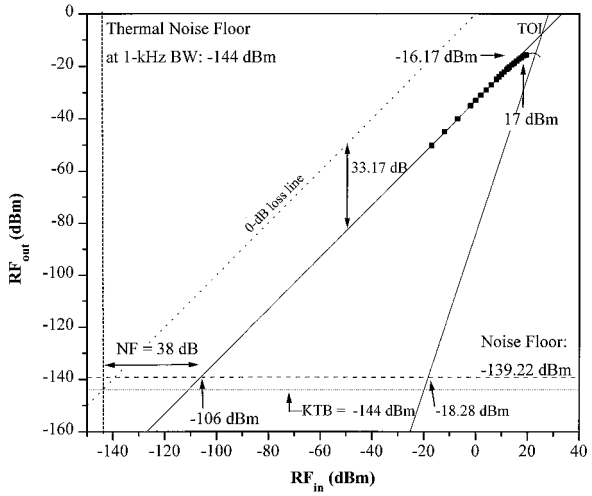

Fig. 7. FO-link fundamental and two-tone intermodulation distortion output versus the link fundamental input at 3 GHz (resolution bandwidth 1 kHz).

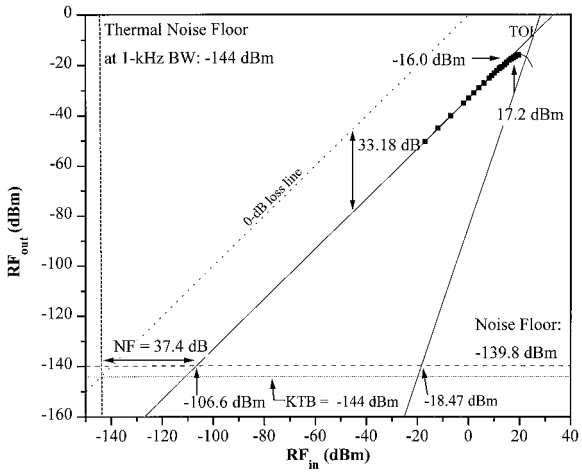

Fig. 9. FO-link fundamental and two-tone intermodulation distortion output versus the link fundamental input at 3 GHz when the dynamic range loss recovery technique is used (resolution bandwidth 1 kHz).

dynamic range compensation technique is used. Again, full dynamic range compensation is obtained with our technique. A CDR of 123 dB·kHz (or 153 dB·Hz) and a SFDR of 88 dB·kHz$^{2/3}$ (or 108 dB·Hz$^{2/3}$) was obtained. The optical attenuator settings used for this experiment were the same as those used in the 6-GHz case. Note that the acquired CDR and SFDR are ~5 dB and ~3 dB lower, respectively, than in the 6-GHz case. This is due to the lower P_{π} of the modulator at 3 GHz and thus to the lower 1-dB compression point at this frequency. Our experiments showed a 1-dB compression input power of 17 dBm, which is ~4 dB lower than the 1-dB compression input power at 6 GHz.

The gain of the FO link was also tested for the 3–6 GHz band. A Hewlett-Packard rf network analyzer (Model HP-8720-D) was used. Figure 10 shows the gain for the 3–6 GHz band for the three different experimental setups. The rf input power of the network analyzer was set at 0 dBm. Figure 10(a) shows the gain for the FO link with the optical attenuator set to give 3 mW of optical power incident onto the photodetector. Figure 10(b) shows the FO link with the PDL and the same setting for the attenuator, and Fig. 10(c) shows the FO link with the PDL and the attenuator set so that the optical power impinging onto the photodetector is again 3 mW. In Fig. 10 it can be seen that the PDL acts only as an attenuator to the FO link. It can be seen from the network analyzer plots that the loss due to the PDL is ~0.6 dB lower for the 3-GHz case than for the 6-GHz case.

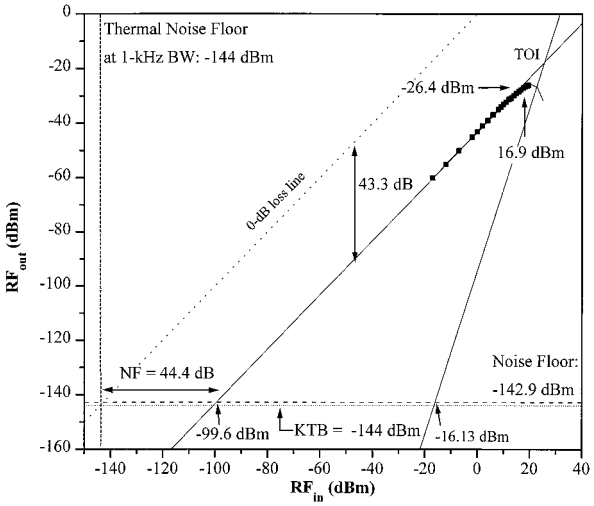

Fig. 8. FO-link fundamental and two-tone intermodulation distortion output versus the link fundamental input at 3 GHz when the PDL is inserted in the optical path (resolution bandwidth 1 kHz).

4. Discussion of Fiber-Optic-Link–Photonic Delay-Line System Performance

The dynamic range recovery technique proposed is easily accomplished, since the available optical power from the diode-pumped Nd:YAG laser is high enough so that after propagation of the optical signal through the FO link and the PDL the optical power impinging onto the fast photodetector is more than what is required from the photodetector for optimum dynamic range. The optical attenuator is used to adjust the optical power at levels acceptable from the photodetector for operation below the saturation and the nonlinear regimes. For example, for a 7-bit PDL with an optical insertion loss of 1.3 dB/bit the total optical insertion loss of the PDL is 7×1.3 dB = 9.1 dB. The optical insertion loss of an external modulator is ~7 dB (~4 dB due to the device loss and 3 dB due to the quadrature bias operation). Thus the total optical insertion loss is 16.1 dB. Additional optical losses due to the fibers interconnecting the laser to the modulator, the modulator to the PDL, and the PDL to the photodetector and due to the fiber connectors can be <1 dB. If a 200-mW diode-pumped laser is used, the optical power available for delivery at the photodetector is 4 mW. This is more than what is required

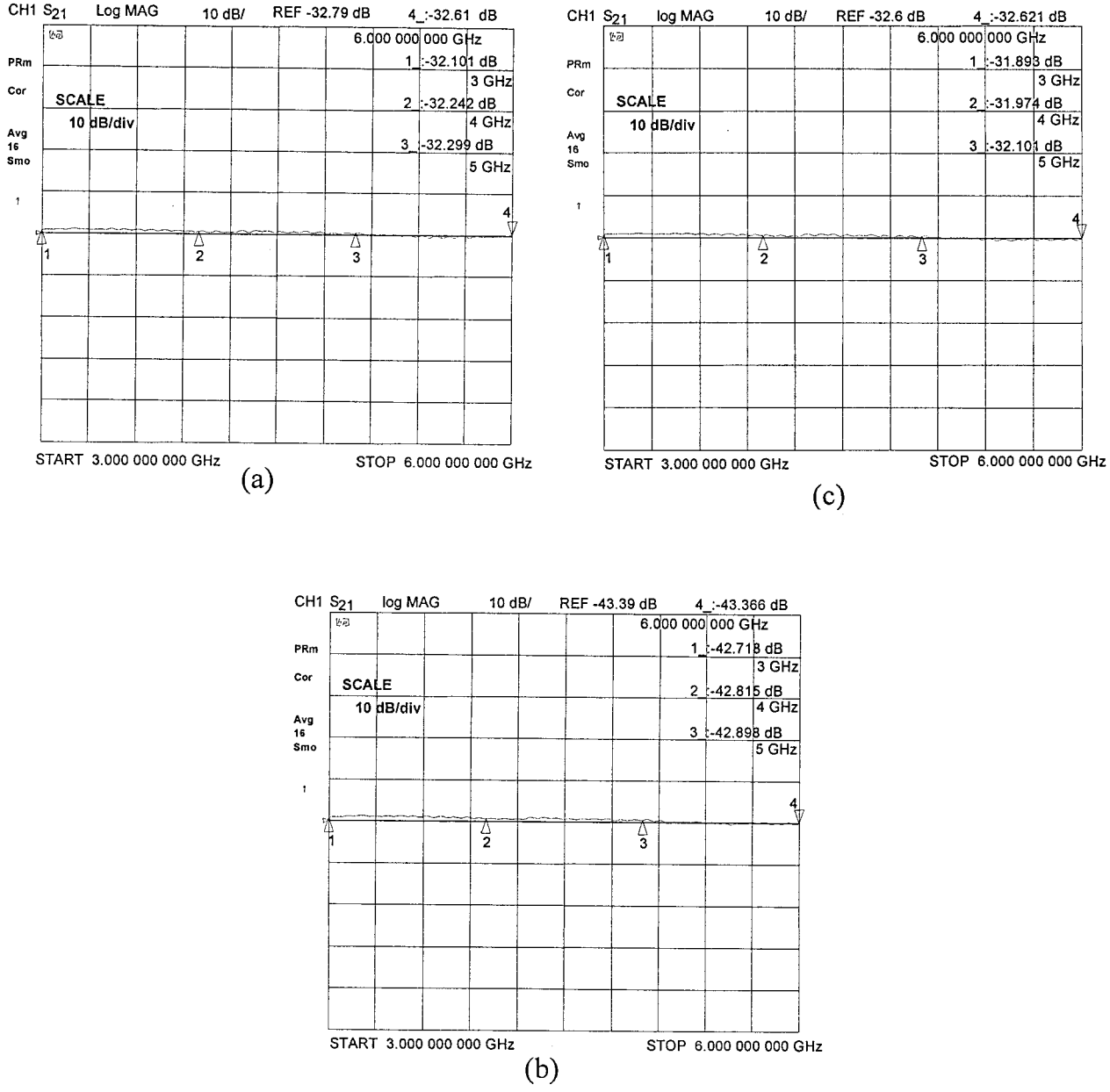

Fig. 10. Network analyzer plots showing the rf gain of the FO link (a) without the PDL, (b) with the PDL, and (c) with the PDL and the dynamic range compensation technique.

by our photodetector for optimum dynamic range. Thus the FO attenuator can be used to adjust the optical power. Note that if our photodetector could handle higher optical powers, the dynamic range would have been higher. Currently, the limited optical power capacity of the photodetectors in the *S* or the *C* band is the limiting factor for much higher dynamic ranges in these bands.

The proposed optical attenuation system does not require a wide range of attenuation levels (i.e., from 0 to >10 dB). Experiments have shown that the within channel PDL bit insertion loss variation due to the optical insertion losses of the optical components is approximately ±0.05 dB.[3] For a 4-bit PDL we measured a ±0.2-dB insertion loss variation.[3] Thus it is expected that for a 7-bit PDL the total insertion loss variation will be approximately ±0.4 dB. Insertion loss variation due to the nonuniformities throughout the entire active area for the optical components are expected to be within ±5% of their specifications in the worst case. This leads to a variation of less than ±0.3 dB. So the worst-case-scenario variation is expected to be ±0.7 dB. Hence the amplitude control system would need to have the capability of 1.4 dB of maximum attenuation. To obtain this 1.4-dB optical attenuation with a resolution of 0.1 dB, a 4-bit binary optical attenuator can be used. Note also that the rf characteristics of the modulator and of the photodetector affect the overall gain of the system and may limit the performance [Fig. 10(a)]. For a completely balanced, flat gain response throughout the entire operational band (e.g., 3–6 GHz) the different rf performance can be calibrated and balanced out by use of the optical attenuation system.

Note that the dominant noise in our FO link is the shot noise, since the relative intensity noise of the diode-pumped laser is approximately −170 dBm/Hz. In our experiment only the input power impinging on the photodetector changes; thus the noise-floor variation in the different experimental cases is dependent on the effect of the optical power on the shot noise. The modulator thermal noise is proportional to the microwave-modulated optical power and becomes significant as the input optical power is increased. Since in our case the optical input power to the modulator is the same, the modulator thermal noise contribution is the same in all the cases. This is why we chose to position the FO attenuator after the modulator and not before it. The rest of the noise contribution comes from the photodetector dark current and the thermal noise that are independent of the optical power.

From the above discussion and from the fact that the FO-link gain increases in proportion to the square of the optical power,[9] whereas the noise floor increases in proportion to the optical power,[9] the FO-link dynamic range can be optimized by adjustment of the optical power. Currently, the limit to further maximization of the CDR and the SFDR in the GHz regime is the inability of the fast photodetectors to handle larger optical powers that could eventually lead to an improved FO-link–PDL system dynamic range and may be in the 3-dB NF limit.[32] Nevertheless, recent results have shown that photodiode nonlinearities can be reduced with increase of the bias,[33] thus promising higher dynamic range. A balanced high-power photodetection scheme has also demonstrated increased dynamic range.[10] We can also achieve increased dynamic range by low biasing the Mach–Zehnder modulator with the penalty of reduced gain, provided that single-octave operation is needed.[34] Optical carrier suppression has also been proposed for improved dynamic range.[35] It has been proposed that this optical carrier suppression can be accomplished entirely within the modulator waveguide circuitry.[36]

5. Conclusion

In conclusion, we have proposed and experimentally demonstrated a dynamic range recovery technique for switched PDL's used for phased-array antenna control applications. This method employs a high-speed variable optical attenuator that operates synchronously with the variable PDL to maintain an optimized optical power level on the output photodetector. We have proposed various optical designs to implement this high-speed attenuator. Dynamic range recovery was demonstrated for a 3-bit PDL with an optical insertion loss of 5.5 dB, fed by a FO link consisting of commercially available components. A compression dynamic range (CDR) of 158 $dB \cdot Hz$ and a noise figure of 36.9 dB were measured for the FO-link–PDL system. The spurious free dynamic range (SFDR) was estimated to be >111 $dB \cdot Hz^{2/3}$. The use of the high-speed optical attenuator also provides the necessary signal calibration for the different PDL settings and channels. Improved overall system dynamic range can be accomplished with lower insertion loss PDL's, optical carrier suppression, low biasing of the electro-optic modulator, and/or photodetectors that can handle larger optical powers.

The authors thank Edward Ackerman of MIT Lincoln Labs for his useful and helpful discussions. This study was supported by grant N000149510988 from the Office of Naval Research.

References

1. N. A. Riza, ed., *Selected Papers on Photonic Control Systems for Phased Array Antennas*, Vol. MS136 of SPIE Milestone Series (SPIE Press, Bellingham, Wash., 1997).
2. N. A. Riza and N. Madamopoulos, "Characterization of a FLC-based time delay unit for phased array antennas," J. Lightwave Technol. **15,** 1088–1094 (1997).
3. N. Madamopoulos and N. A. Riza, "Switched photonic delay line for phased array antenna control using externally modulated microwave fiber-optic link," in *Optical Technology for Microwave Applications*, A. Goutzoulis, ed., Proc. SPIE **3160,** 45–54 (1997).
4. E. Ackerman, C. Cox, and N. A. Riza, Eds., *Selected Papers on Analog Fiber-Optic Links*, Vol. MS149 of SPIE Milestone Series (SPIE Press, Bellingham, Wash., 1998).
5. A. S. Daryoush, E. Ackerman, N. R. Samant, S. Wanuga, and D. Kasemset, "Interfaces for high-speed fiber-optic links: analysis and experiment," IEEE Trans. Microwave Theory Tech. **39,** 2031–2044 (1991).
6. C. Cox III, G. E. Betts, and L. M. Johnson, "An analytic and experimental comparison of direct and external modulation in analog fiber-optic links," IEEE Trans. Microwave Theory Tech. **38,** 501–509 (1990).
7. C. Cox III, E. Ackerman, R. Helkey, and G. E. Betts, "Techniques and performance of intensity-modulation direct-detection analog optical links," IEEE Trans. Microwave Theory Tech. **45,** 1375–1383 (1997).
8. G. E. Betts, C. H. Cox, and K. G. Ray, "20 GHz optical analog link using an external modulator," IEEE Photonics Technol. Lett. **2,** 923–925 (1990).
9. E. Ackerman, S. Wanuga, D. Kasemset, A. S. Daryoush, and N. R. Samant, "Maximum dynamic range operation of microwave external modulation fiber-optic link," IEEE Trans. Microwave Theory Tech. **41,** 1299–1306 (1993).
10. K. J. Williams, L. T. Nichols, and R. D. Esman, "Photodetector nonlinearity limitations on a high-dynamic range 3 GHz fiber-optic link," J. Lightwave Technol. **16,** 192–199 (1998).
11. A. M. Yurek, S. W. Merritt, and G. Drake, "Determining the cascade parameters of externally modulated links," Microwave J. **38,** 80–86 (1995).
12. N. Madamopoulos and N. A. Riza, "Adaptable-delay balanced-loss binary photonic delay line architectures using polarization switching," Opt. Commun. **152,** 135–143 (1998).
13. L. Xu, R. Taylor, and S. R. Forrest, "True time-delay phased-array antenna feed system based on optical heterodyne techniques," IEEE Photonics Technol. Lett. **8,** 160–162 (1996).
14. W. W. Ng, A. A. Walston, G. L. Tangonan, J. J. Lee, I. L. Newberg, and N. Bernstein, "The first demonstration of an optically steered microwave phased array antenna using true-time delay," J. Lightwave Technol. **9,** 1124–1131 (1991).
15. L. Cardone, "Ultra-wideband microwave beamforming technique," Microwave J. **28,** 121–131 (1985).
16. A. P. Goutzoulis, D. K. Davies, and J. M. Zomp, "Hybrid electronic fiber optic wavelength-multiplexed system for true time-

delay steering of phased array antennas," Opt. Eng. **31,** 2312–2322 (1992).
17. H. Zmuda, R. A. Soref, P. Payson, S. Johns, and E. N. Toughlian, "Photonic beamformer for phased array antennas using a fiber grating prism," IEEE Photonics Technol. Lett. **9,** 241–243 (1997).
18. D. Dolfi, F. Michel-Gabriel, S. Bann, and J. P. Huignard, "Two-dimensional optical architecture for time-delay beam forming in a phased-array antenna," Opt. Lett. **16,** 255–257 (1991).
19. R. F. Mathis, W. L. Floyd, and S. A. Pappert, "High performance fiber optic delay line," *Proceedings of the Seventh Annual DARPA Symposium on Photonic Systems for Antenna Applications* (*PSAA-7*), M. L. Van Blaricum, Conference Chair, C. H. Cox III, Program Chair (Defense Advanced Research Projects Agency, Washington, D.C., 1997), pp. 9–14.
20. Optical Variable Attenuator Module, OVA-610, Product Specifications (Santec Corporation, Aichi, Japan, 1998).
21. N. A. Riza, "Advances in three dimensional reversible photonic modules for phased array control," in *Photonics and Radio Frequency*, B. M. Hendrickson, ed., Proc. SPIE **2844,** 274–2283 (1996).
22. S. E. Broomfield, M. A. A. Neil, E. G. S. Paige, and G. G. Yang, "Programmable binary phase-only optical device based on ferroelectric liquid crystal SLM," Electron. Lett. **28,** 26–27 (1992).
23. M. O. Freeman, T. A. Brown, and D. M. Walba, "Quantized complex ferroelectric liquid crystal spatial light modulators," Appl. Opt. **31,** 3917–3929 (1992).
24. J. Kim and N. A. Riza, "Fiber array optical coupling design issues for photonic beamformers," in *Advances in Optical Information Processing VII*, D. R. Pape, ed., Proc. SPIE **2754,** 271–282 (1996).
25. N. A. Riza, and S. Yuan, "Demonstration of a liquid-crystal adaptive alignment tweeker for high-speed infrared band fiber-fed free-space systems," Opt. Eng. **37,** 1876–1880 (1998).
26. V. T. Tondiglia, L. V. Natarajan, R. L. Sutherland, T. J. Bunning, and W. W. Adams, "Volume holographic image storage and electro-optical readout in a polymer-dispersed liquid-crystal film," Opt. Lett. **20,** 1325–1327 (1995).
27. N. A. Riza and S. E. Saddow, "N-bit optically controlled microwave signal attenuator using the photoconductive effect," in *Optical Technology for Microwave Applications VII*, A. P. Goutzoulis, ed., Proc. SPIE **2560,** 9–18 (1995).
28. N. A. Riza and S. E. Saddow, "Optically controlled photoconductive N-bit switched microwave signal attenuator," IEEE Microwave Guid. Wave Lett. **5,** 448–450 (1995).
29. *Designer's Guide to External Modulation*, (Uniphase Telecommunications Products, Electro-Optic Products Division, Bloomfield, Conn., 1997).
30. B. H. Kolner and D. W. Dolfi, "Intermodulation distortion and compression is an integrated electro-optic modulator," Appl. Opt. **26,** 3676–3680 (1987).
31. H. Goldberg, "Some notes on noise figure," Proc. IRE **36,** 1205–1214 (1948).
32. C. Cox, E. Ackerman, and G. Betts, "Relationship between gain and noise figure of an optical analog link," in *IEEE Microwave Theory and Techniques Society Symposium Digest*, R. G. Ranson, ed. (Institute of Electrical and Electronics Engineers, New York, 1996), pp. 1551–1554.
33. K. Williams, R. Esman, and M. Dagenais, "Nonlinearities in p-i-n microwave photodetectors," IEEE Photonics Technol. Lett. **14,** 94–96 (1996).
34. M. L. Farwell, W. S. C. Chang, and D. R. Huber, "Increased linear dynamic range by low biasing the Mach-Zehnder modulator," IEEE Photonics Technol. Lett. **5,** 779–782 (1993).
35. R. D. Esman and K. J. Williams, "Wideband efficiency improvement of fiber optic systems by carrier subtraction," IEEE Photonics Technol. Lett. **7,** 218–220 (1995).
36. G. Drake and B. Merritt, "High-dynamic range applications of integrated optic modulators," in *Optical Technology for Microwave Applications VII*, A. P. Goutzoulis, ed., Proc. SPIE **2560,** 2–8 (1995).